PHYSICAL REVIEW B **73**, 020504(R) (2006)

Phonon-induced quadrupolar ordering of the magnetic superconductor $TmNi_2B_2C$

N. H. Andersen,[1] J. Jensen,[2] T. B. S. Jensen,[1] M. v. Zimmermann,[3] R. Pinholt,[1] A. B. Abrahamsen,[1] K. Nørgaard Toft,[1] P. Hedegård,[2] and P. C. Canfield[4]

[1]*Materials Research Department, Risø National Laboratory, DK-4000 Roskilde, Denmark*

[2]*Niels Bohr Institute, Universitetsparken 5, DK-2100 Copenhagen Ø, Denmark*

[3]*Hamburger Synchrotronstrahlungslabor at Deutsches Elektronen Synchrotron, Notkestrasse 85, 22603 Hamburg, Germany*

[4]*Ames Laboratory and Department of Physics and Astronomy, Iowa State University, Ames, Iowa 50011, USA*

(Received 26 August 2005; published 31 January 2006)

We present synchrotron x-ray diffraction studies revealing that the lattice of thulium borocarbide is distorted below $T_Q \simeq 13.5$ K at zero field. T_Q increases and the amplitude of the displacements is drastically enhanced by a factor of 10 at 60 kOe when a magnetic field is applied along [100]. The distortion occurs at the same wave vector as the antiferromagnetic ordering induced by the *a*-axis field. A model is presented that accounts for the properties of the quadrupolar phase and explains the peculiar behavior of the antiferromagnetic ordering previously observed in this compound.

DOI: 10.1103/PhysRevB.73.020504 PACS number(s): 74.70.Dd, 75.25.+z, 75.80.+q

More than ten years ago it was discovered that four of the rare-earth borocarbides (Tm, Ho, Er, and Dy) show a coexistence of superconductivity and antiferromagnetic ordering with comparable transition temperatures.[1,2] Superconductivity occurs below $T_c = 11$ K and the Néel temperature is $T_N = 1.52$ K in $TmNi_2B_2C$.[3] The characterization and the understanding of these intermetallic compounds have made much progress during the previous decade, as may be seen in a recent review.[4] Although unusual phenomena have been detected, the type-II superconductivity of these materials seems to be described by the BCS theory. The electronic system strongly influences the acoustic and optical Δ_4 phonon branches close to (0.5, 0, 0) and (0, 0.5, 0) in the nonmagnetic Lu and Y versions of these compounds.[5–7] The two vectors connect parallel areas of the Fermi surface,[8] so nesting explains why the electron-phonon interaction is particularly large at these wave vectors. This enhancement of the electron-phonon interaction is probably the primary reason for the relatively high T_c values of the borocarbides. Nesting is generally also assumed to be important for the magnetic susceptibility of the band electrons by causing a maximum in the Ruderman-Kittel-Kasuya-Yoshida (RKKY) coupling of the rare-earth moments at the nesting vectors.[8]

The magnetic properties of $TmNi_2B_2C$ single crystals have been studied by magnetization measurements[9] and by neutron diffraction.[10–12] The ordering vector at zero field is $\boldsymbol{Q}_F = (0.094, 0.094, 0)$ with the magnetic moments transversely polarized along the easy *c* axis. The shift of the magnetic ordering vector away from zero is probably a consequence of the Anderson-Suhl screening of the long-wavelength susceptibility of the superconducting electrons.[11] Applying a field in excess of 10–15 kOe along [100], the magnetic ordering changes into another antiferromagnetic one at the wave vector $\boldsymbol{Q}_A = (0.483, 0, 0)$. In the original experiment, only fields of up to 18 kOe were applied,[11] and the new magnetic phase was considered to be the stable one at zero field in case the electrons were normal, but because the superconducting electrons were more strongly affected by the superzone energy gaps at $\boldsymbol{Q}_A$ than at $\boldsymbol{Q}_F$, the long-wavelength ordering became the favorable one of the combined system at small fields. The extension of the experiment up to a field of 60 kOe clearly showed that this interpretation could not be correct,[12] since the $\boldsymbol{Q}_A$ phase becomes the more stable the higher the field is, and the temperature variation of the magnetization more and more resembles that of the antiferromagnetic order being induced by the uniform field. This highly surprising observation motivated our search for a field-dependent quadrupolar ordering of the system, observable through the accompanying deformation of the lattice.

The experiments were performed at the Hamburger Synchrotronstrahlungslabor, Hamburg, Germany (HASYLAB) using the BW 5 high-energy ($\approx$100 keV) beamline with a triple-axis diffractometer and (1, 1, 1) Si/Ge-gradient crystals as monochromator and analyzer. The single crystal of $TmNi_2B_2C$, grown by the flux method[9] is platelike with an irregular plate shape and approximate dimensions of $4 \times 4 \times 0.8$ mm^3 along the *a*, *b*, and *c* axes, respectively. The crystal was mounted with the *a* and *c* axes in the scattering plane of a horizontal 10 tesla cryomagnet. Geometric constraints required that the field be offset by 5° from the *a* axis in order to probe the expected lattice distortion wave with the symmetry of the Δ_4 phonon mode close to (0.48, 0, 8) along with the (0, 0, 8) Bragg reflection. Temperature- and field-dependent superstructure peaks were found at scattering vector (0.484(2), 0, 8) with the integrated x-ray intensities as shown in Fig. 1. In order to include the intensity from minor satellite crystallites we use numerical summation. The x-ray cross section is completely dominated by the scattering from the Tm ions, and scans performed at (0.484, 0, 0) showed negligible intensity. This is clear evidence for a transverse displacement of the Tm ions along the *c* axis corresponding to the acoustic Δ_4 phonon symmetry. The (0, 0, 8) Bragg reflection was used as a reference for accurate determination of the superstructure peak position and estimates of the superstructure displacement amplitudes. However, the irregular crystal geometry and the small scattering angles result in rather low and uncertain sample transmission coefficients of the order of 4.6×10^{-3} and 8.0×10^{-3} for the (0, 0, 8) and

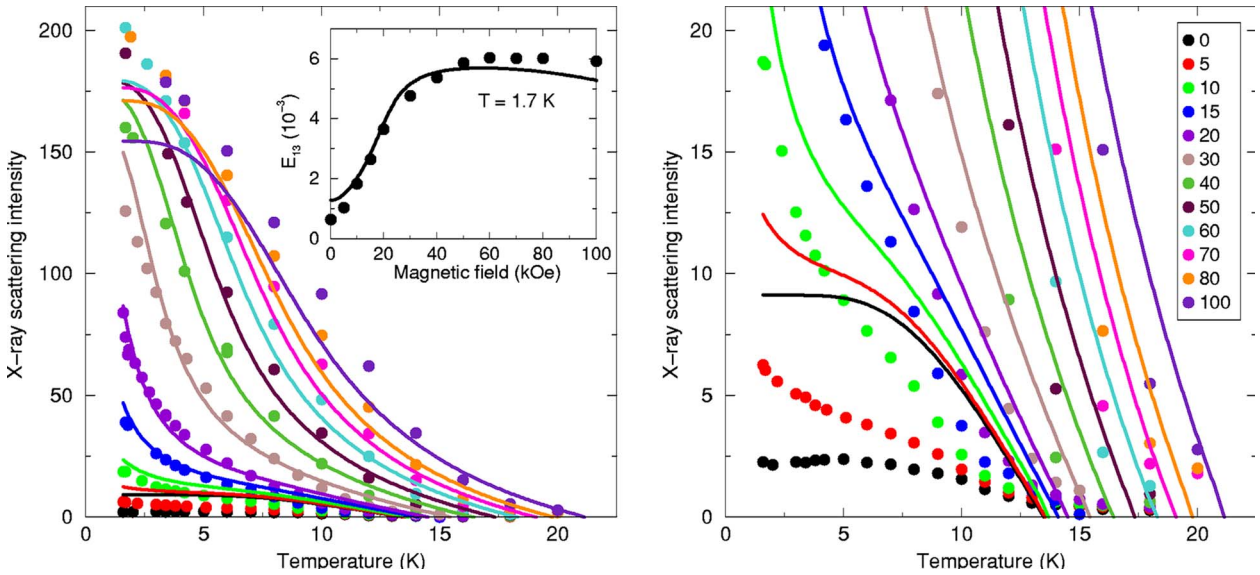

FIG. 1. (Color online) Integrated x-ray scattering intensity at (0.484, 0, 8) as a function of temperature in the presence of an applied field along [100]. The colored symbols used for the different values of the field (in units of kOe) are specified in the legend box. The two figures include the same results, but the intensity scales differ by a factor of 10. The intensity is proportional to the square of the displacement of the Tm ions, and the solid curves show the results derived from the model. The inset shows the field dependence of the strain amplitude E_{13} at 1.7 K derived from the experiments in comparison with the calculated results.

(0.484, 0, 8) reflections, respectively. Including these corrections and defining the strain of the Tm ion at site $\boldsymbol{R}_i$

$$E_{13}(i) = \frac{u_3(\boldsymbol{R}_i)}{a/2} = E_{13}\cos(\boldsymbol{Q}_A \cdot \boldsymbol{R}_i + \phi), \tag{1}$$

we find that the absolute displacements of the Tm ions at 1.7 K and 60 kOe correspond to a strain amplitude of $E_{13} \approx 6 \times 10^{-3}$. The resolution of the diffractometer was determined by the peak profiles of the (0, 0, 8) Bragg peak yielding a crystal mosaicity of $\approx 0.02°$ full width at half maximum (FWHM). The scans along the a axis were essentially rocking curves with Lorentzian profiles while the scans along the c axis were Gaussian shaped. At low temperatures the correlation length along a, corrected for instrumental resolution, is determined to be 185 Å when the quadrupolar phase coexists with the magnetic $\boldsymbol{Q}_F$ phase, and it attains an almost constant value of ≈ 275 Å in the $\boldsymbol{Q}_A$ phase. At zero field and low temperatures the Gaussian peaks in the c direction indicate boxlike structures of lengths ≈ 230 Å that increase to values above the resolution limit of ≈ 300 Å at 100 kOe. The superstructure peak widths are essentially temperature independent at low temperatures but start to broaden when approaching T_Q.

Setting up a model we use the crystal-field (CF) parameters of the Tm ions determined from the observation of CF transitions[13] and from the high-temperature susceptibilities.[9] Here we take into account the anisotropy due to the classical dipole-dipole interaction, $\mathcal{J}_{aa}(\boldsymbol{0}) = \mathcal{J}_{cc}(\boldsymbol{0}) + 9.15$ μeV, adjust the CF parameters accordingly ($B_2^0 = -0.1$, $B_4^0 = 0.000\,33$, $B_4^4 = -0.01$, $B_6^0 = 0.78 \times 10^{-5}$, and $B_6^4 = -1.1 \times 10^{-4}$ in units of meV), and include the demagnetization field in the Zeeman term. The zero-field value of T_N determines the effective two-ion coupling to be $\mathcal{J}_{cc}(\boldsymbol{Q}_F) \simeq 8.7$ μeV, which is also approximately its value at zero wave vector in the normal phase. The purely magnetic part of the Hamiltonian is well characterized, and the additional quadrupolar-magnetoelastic part of the mean-field Hamiltonian is, by symmetry, considered to be

$$\Delta\mathcal{H}(i) = -B_{13}E_{13}(i)O_2^1(i) + c_E E_{13}^2(i) + \tfrac{2}{3}B_E E_{13}^4(i) - K(\boldsymbol{Q}_A)\langle O_2^1(i)\rangle\left[O_2^1(i) - \tfrac{1}{2}\langle O_2^1(i)\rangle\right]. \tag{2}$$

Here $O_2^1(i) = \frac{1}{2}(J_x J_z + J_z J_x)_i$ with x, y, and z along [100], [010], and [001], respectively. $E_{13}(i)$ is determined by minimizing the strain-dependent part of the average free energy

$$\Delta F = -B_{13}E_{13}\langle\langle O_2^1\rangle\rangle + \tfrac{1}{2}c_E E_{13}^2 + \tfrac{1}{4}B_E E_{13}^4, \tag{3}$$

where $\langle\langle O_2^1\rangle\rangle$ is the thermal value $\langle O_2^1(i)\rangle\cos(\boldsymbol{Q}_A \cdot \boldsymbol{R}_i + \phi)$ averaged over the lattice. E_{13} determines $E_{13}(i)$ according to Eq. (1). The transition temperature T_Q of the quadrupolar-ordered phase is independent of the value of the fourth-order elastic constant B_E. It is determined by the effective quadrupolar coupling

$$K_{\text{eff}}(\boldsymbol{Q}_A) = K(\boldsymbol{Q}_A) + \frac{B_{13}^2}{2c_E} \tag{4}$$

being equal to the inverse of the noninteracting quadrupolar susceptibility at the temperature T_Q, or $K_{\text{eff}}(\boldsymbol{Q}_A) = 1/\chi_{O_2^1}(T_Q) = 0.0187$ meV, when assuming $T_Q = 13.5$ K at zero field. The properties of the CF Hamiltonian imply that the quadrupolar susceptibility increases with the a-axis field, and the predicted field dependence of T_Q is in reasonable agreement with observations according to Fig. 1. In the zero-temperature limit $\chi_{O_2^1}$ becomes even more sensitive to the field. Here its maximum value at a field of 20 kOe is nearly

a factor of 3 larger than the zero-field value. Although this increase is large, it is far from explaining the dramatic enhancement of E_{13} observed at 1.7 K (see the inset in Fig. 1). In the nonmagnetic borocarbides, the electron–phonon interaction is close to enforce a complete softening of the Δ_4 phonon mode at the nesting wave vector corresponding to $\boldsymbol{Q}_A$ in the Tm system. The phonon energy is 10 meV at room temperature and about 4 meV at 4.2 K in the Lu compound.[5] In the model above, the effects of the electron-phonon interaction are included in terms of the phenomenological parameters c_E and B_E. If the electron–phonon interaction is as important in the present system as in Lu borocarbide, then c_E should be small, nearly zero, and B_E would be decisive as soon as the lattice distortion becomes nonzero. This is the argument for introducing B_E, which has the additional effect that the two contributions to the effective quadrupolar coupling behave differently. This allows a differentiation between the effects due to B_{13} and those due to the quadrupolar–quadrupolar interaction $K(\boldsymbol{Q}_A)$.

The quadrupolar ordering has the unique consequence (we are not aware of any other systems showing this behavior) that the application of a uniform field induces a modulated magnetic moment perpendicular to the field. This effect was the very reason why we started to look for the quadrupolar ordering, and the explanation for it is straightforward. When $E_{13}(i)$ or $\langle O_2^1(i)\rangle$ is nonzero, the CF Hamiltonian includes an anisotropy term $O_2^1(i)$. This implies that the paramagnetic moment of the ith site induced by an x-axis field is not along the field, but is rotated an angle towards the z axis in proportion to the size of the anisotropy term. Since the anisotropy or $\langle O_2^1(i)\rangle$ is modulated in a sinusoidally way with the wave vector $\boldsymbol{Q}_A$, the z component of the induced moment is going to show the same modulation. The tetragonal symmetry of the system implies that the Hamiltonian also includes the equivalent terms obtained by interchanging x and y in Eq. (2). In the domains in which $\langle O_2^{-1}(i)\rangle$ is ordered with the wave vector $\boldsymbol{Q}_A'=(0,0.484,0)$, the application of a field along [100] does not produce any perpendicular magnetic component, and the quadrupolar order parameter is only weakly changed by the field. This means that the [100] field induces a modulated z-axis moment at the wave vector $\boldsymbol{Q}_A$ but not at $\boldsymbol{Q}_A'$, and it destabilizes the $\boldsymbol{Q}_A'$ domains. Hence, the first circumstance explains the absence of magnetic scattering peaks at $\pm\boldsymbol{Q}_A'$, which is discussed in Refs. 11,12. In the final model, we have introduced one more parameter, namely, the value of $\mathcal{J}_{cc}(\boldsymbol{Q}_A)$. This parameter is not decisive for the magnitude of $\langle J_c(\boldsymbol{Q}_A)\rangle$ (notice that $T_Q \gg T_N$), but is important for E_{13} at the lowest temperatures. The fit is significantly improved when assuming this parameter to be small or, actually, slightly negative. The final model is

$$|B_{13}| = 1.91, \quad c_E = 360, \quad B_E = 4.8 \times 10^7,$$

$$K(\boldsymbol{Q}_A) = 0.0086, \quad \mathcal{J}_{cc}(\boldsymbol{Q}_A) = -0.0029, \tag{5}$$

all in units of meV. The different quantities have been calculated[14] by assuming a commensurable quadrupolar ordering with a period of 25 lattice planes along the a axis, i.e., $\boldsymbol{Q}_A \equiv (0.48,0,0)$. The square of the distortions is observed to

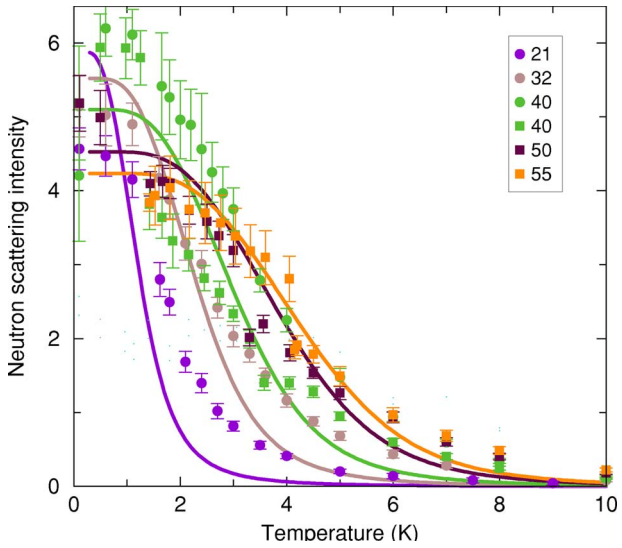

FIG. 2. (Color online) Temperature dependence of the integrated neutron scattering intensity at $\boldsymbol{Q}_A=(0.484,0,0)$ at various values of the applied field along [100] (see Ref. 12). The different values of the field (in units of kOe) are specified in the box. The results were obtained in two different experimental setups (circles and squares). The repetition of the experiment at 40 kOe was used for determining a common scale for the two sets. The intensity is proportional to the squared amplitude of the transverse magnetic moment at the wave vector $\boldsymbol{Q}_A$, and the solid lines are the calculated results.

be a factor of 2 or 3 smaller than calculated at fields below 15 kOe. An equal population of the $\boldsymbol{Q}_A$ and $\boldsymbol{Q}_A'$ domains, at the lowest values of the field, may account for a factor of 2. The model neglects any direct consequences of superconductivity on the magnetic phase diagram, but the x-ray scattering intensities show kinks in their temperature variations at the points where the field is equal to the superconducting critical field H_{c2}. This indicates a (moderate) reduction of the quadrupolar order parameter in the superconducting phase.

The neutron-diffraction results[12] are compared with theory in Fig. 2 assuming that the value of 6 on the intensity scale corresponds to the moment amplitude of $5.0\mu_B$. The calculated amplitudes of the modulation of the moments are of the right order of magnitude. The maximum of the amplitude in the zero-temperature limit is predicted to occur as soon as the system leaves the $\boldsymbol{Q}_F$ phase, at a calculated field of 17 kOe to be compared with an experimental value of 10–15 kOe. The experimental maximum is at about 40 kOe, but we have to remark that there are relatively large, unexplained scatters in the experimental results. Instead of focusing on the discrepancies we emphasize the ability of the present model to account for the highly disparate variations of the properties of the system. Using a simple elastic model we estimate that c_E=360 meV corresponds to an acoustic phonon mode at 2.4 meV close to the soft phonon energy of 4 meV observed in the Lu compound. The value of B_E also appears to be acceptable. The entropy of the electron–phonon system has nearly vanished and the electron–phonon parameters c_E and B_E are expected, as assumed, to stay practically constant below 20 K. Because of the small nonmagnetic entropy, the heat capacity anomaly at T_Q is expected to

be weak, since the CF contribution of the $4f$ electrons is negligible (the ground-state doublet remains degenerate at zero field).

The analysis indicates that the electron–phonon system in $TmNi_2B_2C$, as in the Lu compound, is very close to the point of a lattice instability. In $TmNi_2B_2C$ the transition is occurring because of the additional contributions of magnetoelastic and quadrupolar–quadrupolar interactions. The magnetoelastic interaction derives from the electrical crystal field produced by the displacements of the ions, whereas the quadrupolar–quadrupolar interaction may be mediated by the same charge-density wave responsible for the strong electron–phonon interaction, and, hence, may be an additional consequence of the Fermi-surface nesting. One of the surprises of the present analysis is that the RKKY-exchange interaction does not seem to be much influenced by the nesting since the interaction is found to be much smaller at the nesting wave vector than at $\boldsymbol{Q}_F$.

In conclusion, the x-ray experiments exposed the presence of a quadrupolar phase in $TmNi_2B_2C$ below 13.5 K at zero field. The transition temperature increases and the accompanying deformation of the lattice is grossly enhanced when a field is applied along [100]. From the model analysis we conclude that this occurs mainly because the lattice is already close to the critical point due to the nonmagnetic electron–phonon interaction. The magnetic interactions are the final ingredients that enforce the system to enter the quadrupolar phase, and the analysis indicates that the magnetoelastic crystal field and the quadrupolar–quadrupolar interactions are of nearly equal importance, $K(\boldsymbol{Q}_A)=0.46K_{\mathrm{eff}}(\boldsymbol{Q}_A)$. The quadrupolar ordering has the unique effect that a field applied along [100] induces antiferromagnetic ordering at the same wave vector as the quadrupolar ordering. The Fermi-surface nesting is presumably important for the strong electron–phonon interaction at $\boldsymbol{Q}_A$, and possibly also for the quadrupolar–quadrupolar interaction. Contrary to this, the RKKY interaction is concluded to be relatively weak at this wave vector. This suggests that those electrons that are close to the nesting areas and important for creating the superconducting phase are not the same as those determining the RKKY interaction. The present discovery has basic consequences for understanding the magnetism of borocarbides, and opens up a number of questions. Is there a strain-charge quadrupolar phase in the nonmagnetic borocarbides or a magnetic quadrupolar phase in the other magnetic ones? Previous experiments have not revealed such an effect, but our results motivate a specific reexamination of the other rare-earth materials for the similar deformation we observed in the thulium system. Is the quadrupolar interaction the reason for the longitudinal polarization[15] of the antiferromagnetic ordered moments in the Tb compound? The strong peak at (0.55, 0, 0) in the exchange interaction of the Er compound[16,17] might be another consequence of a quadrupolar interaction rather than the RKKY, but our recent measurements[18] have not indicated any sign of the quadrupolar ordering in this compound.

This work was supported by the Danish Technical Research Council under the Framework Programme on Superconductivity and the Danish Natural Science Council under Dansync and DanScatt. P.C.C. is supported by the Director of Energy Research, Office of Basic Energy Science under Contract No. W-7405-Eng.-82.

[1] R. Nagarajan, C. Mazumdar, Z. Hossain, S. K. Dhar, K. V. Gopalakrishnan, L. C. Gupta, C. Godart, B. D. Padalia, and R. Vijayaraghavan, Phys. Rev. Lett. **72**, 274 (1994).

[2] R. J. Cava *et al.*, Nature (London) **367**, 252 (1994).

[3] R. Movshovich *et al.*, Physica C **227**, 381 (1994).

[4] C. Mazumdar and R. Nagarajan, Curr. Sci. **88**, 83 (2005).

[5] P. Dervenagas, M. Bullock, J. Zarestky, P. Canfield, B. K. Cho, B. Harmon, A. I. Goldman, and C. Stassis, Phys. Rev. B **52**, R9839 (1995).

[6] H. Kawano, H. Yoshizawa, H. Takeya, and K. Kadowaki, Phys. Rev. Lett. **77**, 4628 (1996).

[7] M. Bullock, J. Zaretsky, C. Stassis, A. Goldman, P. Canfield, Z. Honda, G. Shirane, and S. M. Shapiro, Phys. Rev. B **57**, 7916 (1998).

[8] S. B. Dugdale, M. A. Alam, I. Wilkinson, R. J. Hughes, I. R. Fisher, P. C. Canfield, T. Jarlborg, and G. Santi, Phys. Rev. Lett. **83**, 4824 (1999).

[9] B. K. Cho, M. Xu, P. C. Canfield, L. L. Miller, and D. C. Johnston, Phys. Rev. B **52**, 3676 (1995).

[10] B. Sternlieb *et al.*, J. Appl. Phys. **81**, 4937 (1997).

[11] K. Nørgaard, M. R. Eskildsen, N. H. Andersen, J. Jensen, P. Hedegard, S. N. Klausen, and P. C. Canfield, Phys. Rev. Lett. **84**, 4982 (2000).

[12] K. Nørgaard Toft, A. B. Abrahamsen, M. R. Eskildsen, K. Lefmann, N. H. Andersen, P. Vorderwisch, P. Smeibidl, M. Meissner, and P. C. Canfield, Phys. Rev. B **69**, 214507 (2004).

[13] U. Gasser *et al.*, Z. Phys. B **101**, 345 (1996).

[14] J. Jensen and A. R. Mackintosh, *Rare Earth Magnetism: Structures and Excitations* (Clarendon Press, Oxford, 1991).

[15] P. Dervenagas, J. Zaretsky, C. Stassis, A. I. Goldman, P. C. Canfield, and B. K. Cho, Phys. Rev. B **53**, 8506 (1996).

[16] A. Jensen *et al.*, Phys. Rev. B **69**, 104527 (2004).

[17] J. Jensen, Phys. Rev. B **65**, 140514(R) (2002).

[18] N. H. Andersen *et al.* (unpublished).